

# Synthesis Method for Obtaining Characteristic Modes of Multi-Structure Systems

Chenbo Shi, Xin Gu, Shichen Liang, Jin Pan and Le Zuo

**Abstract**—This paper introduces an efficient method of characteristic mode decomposition for multi-structure systems. Our approach leverages the translation and rotation matrices associated with vector spherical wavefunctions, enabling the synthesis of a total system’s characteristic modes through independent simulation of each constituent structure. We simplify the computationally demanding translation problem by dividing it into three manageable sub-tasks: rotation, z-axis translation, and inverse rotation, which collectively enhance computational efficiency. Furthermore, this method facilitates the exploration of structural orientation effects without incurring additional computational overhead. To demonstrate the effectiveness of our approach, we present a series of compelling numerical examples that not only validate the accuracy of the method but also highlight its significant advantages.

**Index Terms**—The theory of characteristic modes, synthesis of characteristic modes, transition matrix, scattering matrix, fast evaluation of characteristic modes.

## I. INTRODUCTION

THE theory of characteristic modes is pivotal in antenna analysis and design [1]–[3]. Its derived form—substructure characteristic modes theory—has gained prominence for revealing the intrinsic electromagnetic properties of structures within complex environments [4]–[6]. This approach is increasingly employed in designing antennas for handheld devices and platform-mounted systems [7]. Recent extensions have unified various characteristic mode formulations, which were traditionally based on the method of moments (MoM), into a more robust scattering-based framework, significantly enhancing numerical efficiency [8], [9]. Despite these advancements, the computational burdens for systems with multiple structures, such as antenna arrays, remain substantial.

In the unified framework [8], [9], characteristic modes are obtained by eigenvalue decomposition of the transition matrix (T-matrix) or scattering matrix. This matrix serves as an operator that connects the incident and structural scattering responses, solely determined by the properties of the structures within a designated enclosing sphere. This characteristic indicates the possibility to construct the T-matrix for combined structures from independent structural data, thus facilitating the rapid computation of characteristic modes for complex

systems. This paper primarily focuses on optimizing and exploring this potential.

Although extensive research in fields such as optical scattering has effectively elucidated and summarized the technique of deriving the total system’s T-matrix from the individual structures’ T-matrices [10]–[13], particularly through employing the two translation properties of spherical wavefunctions [14], [15], we revisit this established method from a unique perspective. We have developed a fully matrixized representation that is not only concise and efficient but also facilitates easier understanding compared to conventional series representations. This is particularly advantageous in scenarios that require specifying the radiation background for characteristic mode decomposition, where our approach minimizes repetitive computations. Following the method outlined in [16], we decompose the general translation problem into three sub-steps: rotation, z-axis translation, and inverse rotation, eschewing the direct solutions typically employed in conventional studies. This significantly curtails computation time, as z-axis translations are inherently simpler. Moreover, by adjusting the translation direction using the rotation matrix, we can correlate problems that have identical translation distances but different directions—common in uniformly arranged structures—thereby enhancing the reuse of the translation matrix and further boosting computational efficiency.

The integration of the rotation matrix within our method introduces additional degrees of freedom; notably, it enables alterations to the structure’s orientation during post-processing, obviating the need to recompute the T-matrix. This enhancement is crucial for investigating the effects of the structure’s posture or polarization. To substantiate our approach, we present a series of illustrative numerical examples that demonstrate the substantial advantages of our synthesis technique in deriving characteristic modes. These examples highlight the potential applications of our method in complex structures and antenna arrays.

## II. UNIFIED THEORY OF CHARACTERISTIC MODES

As a crucial foundation for this paper, this section provides a concise review of the latest developments in characteristic mode theory, equipping the reader with the theoretical framework utilized herein.

The unified theory of characteristic modes articulates its foundational equation through the scattering matrices of structures [9]:

$$\mathbf{SS}_b^\dagger \mathbf{f}_n = s_n \mathbf{f}_n \text{ or } \frac{1}{2} \left( \mathbf{SS}_b^\dagger - \mathbf{1} \right) \mathbf{f}_n = t_n \mathbf{f}_n. \quad (1)$$

Manuscript received Sep. 24, 2024. This work was supported by the Aeronautical Science Fund under Grant ASFC-20220005080001. (Corresponding author: Jin Pan.)

Chenbo Shi, Xin Gu, Shichen Liang and Jin Pan are with the School of Electronic Science and Engineering, University of Electronic Science and Technology of China, Chengdu 611731 China (e-mail: chenbo\_shi@163.com; xin\_gu04@163.com; lscstu001@163.com; panjin@uestc.edu.cn).

Le Zuo is with The 29th Research Institute of China Electronics Technology Group Corporation (e-mail: zorro1204@163.com)

Given the relationships  $\mathbf{S} = \mathbf{1} + 2\mathbf{T}$  and  $\mathbf{S}_b = \mathbf{1} + 2\mathbf{T}_b$ , (1) can be reformulated as

$$(\mathbf{T} + \mathbf{T}_b^\dagger + 2\mathbf{T}\mathbf{T}_b^\dagger) \mathbf{f}_n = t_n \mathbf{f}_n. \quad (2)$$

Here,  $\mathbf{f}_n$  denotes the expansion coefficients of the 4-type (outgoing) spherical wavefunctions for the  $n$ -th characteristic radiation field,  $\mathbf{T}_b$  represents the background's T-matrix, and  $\mathbf{T}$  corresponds to the total system's T-matrix, encompassing both the key and background structures.

The presence of a background structure  $\Omega_b$  allows (2) to solve for the characteristic mode of the key structure  $\Omega_k$  within an environment inclusive of  $\Omega_b$ . This scenario is often referred to as the "substructure characteristic mode". The most basic form occurs when  $\mathbf{T}_b = \mathbf{0}$ , in which case (2) solves for the characteristic mode of the structure radiating in free space.

The algebraic connection between (2) and the MoM is derived from pre-assuming wavefunctions based on real spherical harmonics {cf. [17] for definitions of these wavefunctions}:

$$\mathbf{T} = -\mathbf{P}\mathbf{Z}^{-1}\mathbf{P}^t, \quad \mathbf{T}_b = -\mathbf{P}_b\mathbf{Z}_b^{-1}\mathbf{P}_b^t \quad (3)$$

where  $\mathbf{P}$  and  $\mathbf{P}_b$  are matrices that relate the equivalent electromagnetic currents to their respective radiation fields. While this paper discards the traditional MoM equations, (3) remains instrumental for calculating the T-matrix. The differences of different characteristic mode formulations are explored in greater detail in [8], [9]—with solutions based on (2) generally showing superior performance.

### III. SYNTHESIS OF THE T-MATRIX FOR MULTI-STRUCTURE SYSTEMS

In applications involving multiple structures, calculating the T-matrix of the total system using (3) can be burdensome. However, it is possible to synthesize the system T-matrix using individual structure T-matrices, somewhat akin to domain decomposition methods. The T-matrix maps the 1-type spherical wavefunction coefficients  $\mathbf{a}$  of incident waves to the 4-type coefficients  $\mathbf{f}$  of radiating (scattering) waves, *i.e.*,  $\mathbf{f} = \mathbf{T}\mathbf{a}$ . This allows for an understanding of the system's T-matrix in relation to its components through a scattering-problem perspective.

Assuming the system comprises  $M$  structures, labeled as  $p = 1, 2, \dots, M$  (see Fig. 1), the system generates a scattering wave  $\mathbf{f}$  under an external incident wave  $\mathbf{a}$ . From the perspective of the  $p$ -th structure (using its local coordinate system), the contribution to the scattering wave reads

$$\mathbf{f}^p = \mathbf{T}^p \mathbf{a}^p. \quad (4)$$

The incident wave  $\mathbf{a}^p$  for the  $p$ -th structure comprises a direct component from  $\mathbf{a}$  (denoted by  $\mathbf{a}_d^p$ ), and scattering contributions  $\mathbf{f}^q$  from other structures ( $q \neq p$ ). By translating  $\mathbf{f}^q$  into the  $p$ -th local coordinate system, we express it as:

$$\mathbf{a}^p = \mathbf{a}_d^p + \sum_{q \neq p} \mathbf{y}_{pq}^t \mathbf{f}^q \quad (5)$$

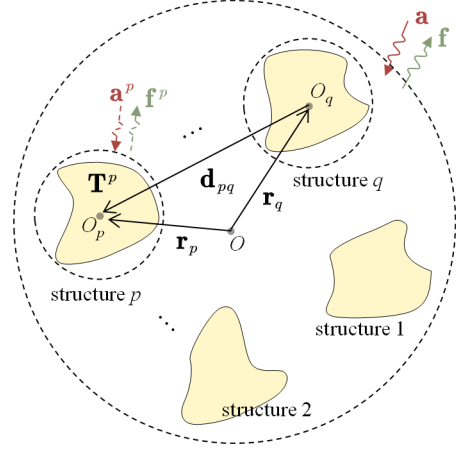


Fig. 1. Schematic of electromagnetic scattering for a multi-structure system.

where  $\mathbf{y}_{pq}$  represents the translation matrix. Substituting this into (4), we obtain

$$\mathbf{f}^p = \mathbf{T}^p \mathbf{a}_d^p + \mathbf{T}^p \sum_{q \neq p} \mathbf{y}_{pq}^t \mathbf{f}^q. \quad (6)$$

If we further transform (6) into matrix form, we have

$$\tilde{\mathbf{f}} = \tilde{\mathbf{T}} \tilde{\mathbf{a}}_d + \tilde{\mathbf{T}} \tilde{\mathbf{y}} \tilde{\mathbf{f}}. \quad (7)$$

This leads to

$$\tilde{\mathbf{f}} = (\mathbf{1} - \tilde{\mathbf{T}} \tilde{\mathbf{y}})^{-1} \tilde{\mathbf{T}} \tilde{\mathbf{a}}_d \quad (8)$$

where

$$\tilde{\mathbf{f}} = \begin{bmatrix} \mathbf{f}^1 \\ \vdots \\ \mathbf{f}^M \end{bmatrix}, \quad \tilde{\mathbf{a}}_d = \begin{bmatrix} \mathbf{a}_d^1 \\ \vdots \\ \mathbf{a}_d^M \end{bmatrix}, \quad \tilde{\mathbf{y}} = \begin{bmatrix} \mathbf{0} & \mathbf{y}_{12}^t & \cdots & \mathbf{y}_{1M}^t \\ \mathbf{y}_{21}^t & \mathbf{0} & \cdots & \mathbf{y}_{2M}^t \\ \vdots & \cdots & \ddots & \vdots \\ \mathbf{y}_{M1}^t & \mathbf{y}_{M2}^t & \cdots & \mathbf{0} \end{bmatrix}$$

and  $\tilde{\mathbf{T}} = \text{diag}(\mathbf{T}^1, \mathbf{T}^2, \dots, \mathbf{T}^M)$ .

For the moment we have successfully represented the radiated fields generated by each structure within their respective local coordinate systems. To determine the T-matrix for the total system, we must correlate these localized quantities into the global coordinate system. This necessitates the introduction of another translation matrix,  $\mathcal{R}_p$ , leading to  $\mathbf{a}_d^p = \mathcal{R}_p^t \mathbf{a}$  and

$$\mathbf{f} = \sum_p \mathcal{R}_p \mathbf{f}^p.$$

In matrix form, this can be simplified to

$$\mathbf{f} = \tilde{\mathcal{R}} \tilde{\mathbf{f}}, \quad \tilde{\mathbf{a}}_d = \tilde{\mathcal{R}}^t \mathbf{a} \quad (9)$$

where  $\tilde{\mathcal{R}} = [\mathcal{R}_1, \mathcal{R}_2, \dots, \mathcal{R}_M]$ .

By substituting (9) into (8) and comparing with the expression  $\mathbf{f} = \mathbf{T}\mathbf{a}$ , we can derive the system T-matrix:

$$\mathbf{T} = \tilde{\mathcal{R}} (\mathbf{1} - \tilde{\mathbf{T}} \tilde{\mathbf{y}})^{-1} \tilde{\mathcal{R}}^t. \quad (10)$$

Note that details regarding the translation matrices  $\mathbf{y}$  and  $\mathcal{R}$  will be discussed in the upcoming section.

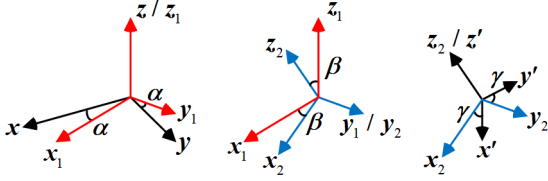


Fig. 2. Euler rotation sequence. The coordinate system  $(x', y', z')$  is derived by initially rotating the  $(x, y, z)$  system about the  $z$ -axis by angle  $\alpha$ , subsequently about the  $y_1$ -axis by angle  $\beta$ , and finally about the  $z_2$ -axis by angle  $\gamma$ .

Through carefully examining each matrix in (10), we can see that the T-matrix of the total system is synthesized from the T-matrices of its constituent structures independently, along with translation matrices that relate solely to positional topology. Notably, this approach does not introduce any additional information about mutual couplings between different structures; these couplings are inherently captured by the spherical wavefunctions, which represents a significant advantage of this theory. In contrast to conventional methods for obtaining the T-matrix of multiple structures, our formulation (10) is fully matrixized, easier to implement, and computationally efficient (see Sec. V for data support of this conclusion).

Another essential task is to determine the T-matrix of the background,  $\mathbf{T}_b$ . This is synthesized using the T-matrices of the remaining structures after excluding the key structures. The process is similar to the one described above, with the primary difference being the removal of matrix blocks associated with the key structures. If we prioritize computing the background  $\mathbf{T}_b$ , the total system T-matrix can then be obtained via the Schur complement method (cf. appendix A), which eliminates much of the redundant computation.

#### IV. TRANSLATION AND ROTATION MATRIX FOR SPHERICAL WAVEFUNCTIONS

In this section, we explore the methods for computing the translation matrices  $\mathcal{Y}_{pq}$  and  $\mathcal{R}_p$ . Both matrices are functions related to the electrical translation distance, *i.e.*,  $\mathcal{Y}_{pq} = \mathcal{Y}(k\mathbf{d}_{pq})$ ,  $\mathcal{R}_p = \mathcal{R}(k\mathbf{r}_p)$ , with  $\mathcal{R} = \text{Re}\{\mathcal{Y}\}$ . Here,  $\mathcal{Y}$  matrix translates 4-type spherical wavefunctions to 1-type, whereas  $\mathcal{R}$  handles translations among the same type of spherical wavefunctions. This underpins the use of  $\mathcal{Y}_{pq}$  in (5)—to translate the scattering wave (4-type) into the incident wave (1-type).

Representations for  $\mathcal{Y}(k\mathbf{d})$  can be found in existing literature. A notable simplification occurs when  $\mathbf{d}$  is parallel to the  $z$ -axis, where  $\mathcal{Y}(k\mathbf{d})$  becomes diagonal in the  $m$ -index (azimuthal angle index). The appendix in [9] provides an efficient formula that significantly reduces computation time for these cases. However, when  $\mathbf{d}$  is not parallel to the  $z$ -axis, the computations become complex and resource-intensive. To address this, we introduce the rotation matrix of the wavefunctions, which reorients the translation problem from a general direction to alignment along the  $z$ -axis, thereby simplifying the computational process.

Any rotation of the coordinate system can be described using Euler angles  $(\alpha, \beta, \gamma)$ , where  $\alpha$  is an azimuthal rotation about the  $z$ -axis, succeeded by a polar rotation  $\beta$  about the

newly oriented  $y$ -axis, and another azimuthal rotation  $\gamma$  about the newly oriented  $z$ -axis, as illustrated in Fig. 2. We can link the spherical wave expansion vectors  $\mathbf{a}/\mathbf{f}$  in the  $(x, y, z)$  coordinate system to  $\mathbf{a}'/\mathbf{f}'$  in the  $(x', y', z')$  coordinate system using a rotation matrix  $\mathcal{D} = \mathcal{D}(\alpha, \beta, \gamma)$  (cf. appendix B for its definition) as:

$$\mathbf{f}' = \mathcal{D}\mathbf{f}, \mathbf{a}' = \mathcal{D}\mathbf{a} \text{ or } \mathbf{f} = \mathcal{D}^t\mathbf{f}', \mathbf{a} = \mathcal{D}^t\mathbf{a}'. \quad (11)$$

Note that  $\mathcal{D}^{-1} = \mathcal{D}^t$ .

By aligning the  $z$ -axis with  $\mathbf{d}$ , we transform the general translation problem into a  $z$ -axis translation problem. The rotation angles  $\alpha$  and  $\beta$  correspond to the azimuthal and polar angles of the spherical coordinates of  $\mathbf{d}$ , respectively, and  $\gamma = 0$ . After performing the  $z$ -axis translation, we revert to the original coordinate system through an inverse rotation to resolve the original translation problem. Therefore, we can deduce that

$$\mathcal{Y}(k\mathbf{d}) = \mathcal{D}^t\mathcal{Y}^z(kd)\mathcal{D} \quad (12)$$

where  $\mathcal{Y}^z(kd)$  is defined as equation (63) in [9], referring to translations along the  $z$ -axis by distance  $d$ .

This approach substantially reduces computational time (*e.g.*, computation time is reduced from 30s to 1.2s for a 646-dimensional translation problem, and from 124s to 2.6s for a 1056-dimensional translation problem) because calculating the rotation matrix takes negligible time. Moreover, the rotation matrix is frequency-independent and can be pre-stored, which allows only the translation matrix to be recalculated for different frequencies. For uniformly arranged arrays, where the translation distances remain constant,  $\mathcal{Y}^z(kd)$  needs to be calculated only once. The translation directions are then adjusted by altering the rotation matrix in (12), further reducing computational burdens.

Additionally, the rotation matrix offers another advantage: obtaining the T-matrix of the structure post-rotation. This concept is analogous to the previous discussion, and the result can be succinctly expressed as

$$\mathbf{T}' = \mathcal{D}^t\mathbf{T}\mathcal{D} \quad (13)$$

where  $\mathbf{T}'$  is the transition matrix for the rotated structure. (13) provides a new degree of freedom to examine the effects of orientation changes of units within the system, without requiring additional electromagnetic simulations.

#### V. NUMERICAL RESULTS: CHARACTERISTIC MODES FOR MULTI-STRUCTURE SYSTEMS

##### A. Dipole near a sphere

To demonstrate the advantages of our synthetic approach in calculating characteristic modes, we analyze the behavior of modes in a dipole-sphere model, as depicted in Fig. 3. Given that the sphere's T-matrix has analytical expressions {cf. §8 of [17]}, we only perform a full-wave simulation for the dipole.

Figure 4 displays the distribution of the eigentrace  $|t_n|$  (also known as the modal significance coefficient) when the sphere's diameter  $2A = L$ . These synthetic results align perfectly with those from full-wave simulations. The eigentraces merge the modal characteristics of both the dipole and the sphere, as in this example, they are specified to radiate in free space.

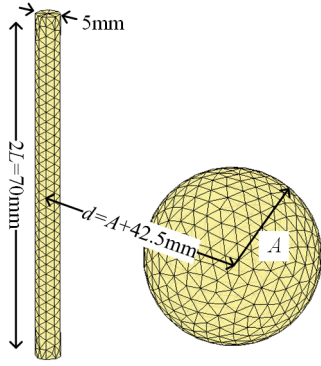


Fig. 3. Dipole-sphere model composed of perfect electric conductor (PEC).

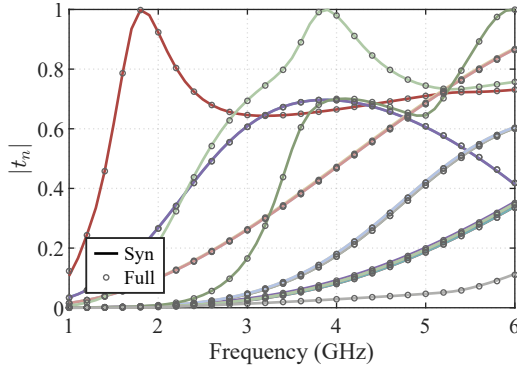


Fig. 4. Eigentraces for the dipole-sphere structure radiating in free space. Data labeled “Syn” were derived using the synthesis method discussed in Section III; “Full” represents results from full-wave simulation.

However, our primary interest lies in scenarios where the dipole radiates near the sphere, as depicted by the dashed line in Fig. 5. In this setup, the eigentraces simplify, predominantly demonstrating the dipole’s radiation against the sphere and filtering out the direct response of the sphere. With the dipole aligned vertical to the sphere, the eigentraces alter slightly compared to when it is parallel to the sphere (referred to as the “horizontal” configuration), as shown by the solid line in Fig. 5. Our synthesized results consistently match those of the full-wave simulations, regardless of the configuration. It’s notable that recalculating the T-matrix for the vertical dipole is unnecessary; it can be derived from the horizontal cases using (13). This allows for easy exploration of other dipole polarizations, though it is not pursued here.

Figure 6 demonstrates the main-mode radiation patterns for the two aforementioned configurations, closely matching the full-wave simulation results. This not only further validates our method but also uncovers new potential applications. Since the T-matrix of the sphere is analytical, increasing its diameter does not significantly add to the computational burden. This capability enables us to consider ground effects for structures near the ground (viewing the Earth as a sphere, for instance). For example, in the configuration shown in Fig. 4, as the sphere’s diameter increases, the directivity of the horizontal dipole enhances while the backward radiation diminishes, aligning with engineering intuition. Conversely, for a vertical dipole, the maximum radiation initially tilts towards the sphere before gradually shifting away, as illustrated in Fig. 7.

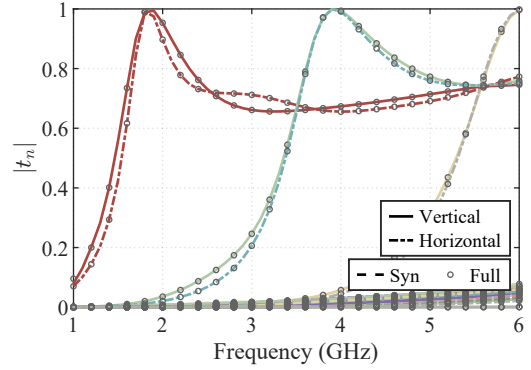


Fig. 5. Eigentraces for the dipole radiating against the sphere structure. “Vertical” indicates the dipole is perpendicular to the sphere, and “horizontal” signifies it is parallel to the sphere.

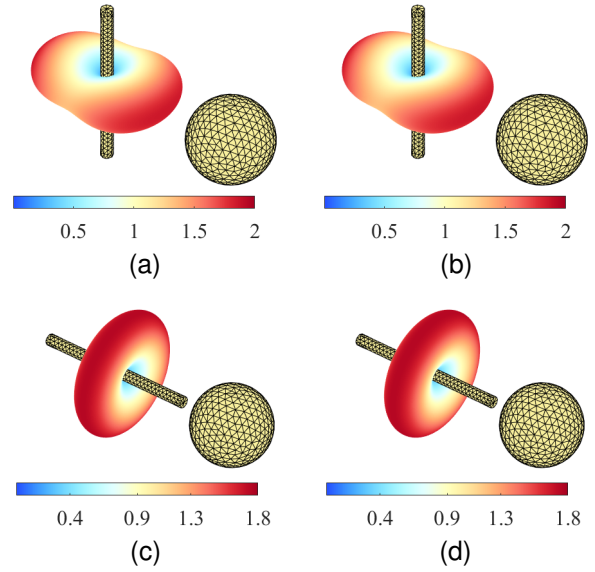


Fig. 6. Radiation pattern of the main mode at 1.7 GHz. Panels (a) and (b) depict the horizontal case, while (c) and (d) show the vertical case. The left panel in each pair is obtained through full-wave simulation, and the right panel through synthesis method. In this figure, the sphere diameter is  $2A = L$ .

### B. 3-cell uniform array

Another illustrative example, depicted in Fig. 8, considers a uniform 3-cell array consisting of open circuit metal rings printed on a substrate. Following the method proposed in section III, we obtain the eigentraces of the characteristic modes, as shown in Fig. 9. Here, three distinct eigentraces cluster near each  $|t_n| = 1$ , reflecting the mode responses of the entire array in free space, with each cell directly contributing to the collective behavior.

Figure 10 showcases the radiation patterns of the first two modes at 4.1 GHz, illustrating that despite similar resonant ( $|t_n| = 1$ ) frequencies, their radiation characteristics differ markedly. The results from our synthetic approach consistently align with those from full-wave simulations in terms of both eigentraces and radiation patterns. Nevertheless, the computational demands of these methods vary significantly. For instance, the full-wave calculation employs equation (2) to determine the total system T-matrix, utilizing 3420 RWG

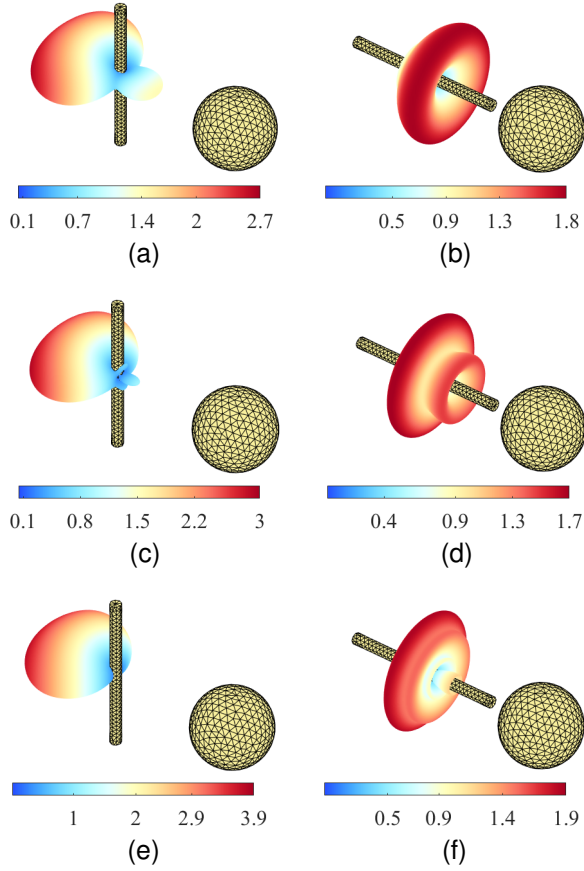


Fig. 7. Radiation patterns. Panels (a), (c), and (e) represent the horizontal case, while (b), (d), and (f) represent the vertical case. The top panel features a sphere diameter of  $2A = 2L$ , the middle panel  $2A = 4L$ , and the bottom panel  $2A = 10L$ . Note that structural changes in the sphere are not depicted in this figure; the structure illustrated is schematic only.

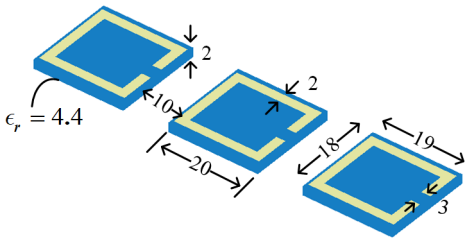


Fig. 8. A 3-cell uniform array model with structure dimensions provided in millimeters.

basis functions per cell to compute the impedance matrix and 646 spherical wavefunctions to expand the electromagnetic field, requiring a total of 83s. In contrast, the synthetic method completes in only 16s, with 11s dedicated to calculating the T-matrix of one cell. When the number of cells increases to five, the full-wave calculation escalates to over 300s, whereas the synthetic method requires merely 24s.

In a subsequent analysis, we modify the setup in Fig. 8 by designating the cells on both sides as radiation background. The resultant eigentraces, displayed as a solid line in Fig. 11, show only two modes resonating within the specified frequency band. Compared to the eigentrace of a single cell in free space (dashed line), the main-mode bandwidth of the array

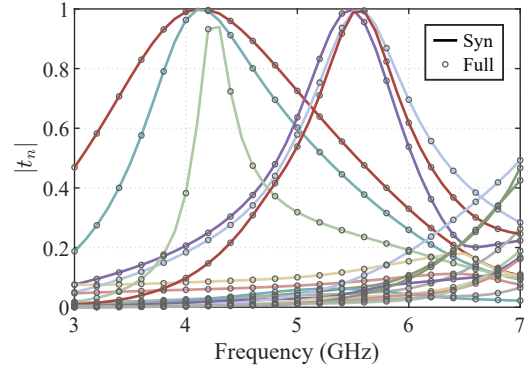


Fig. 9. Eigentraces for the 3-cell array radiating in free space.

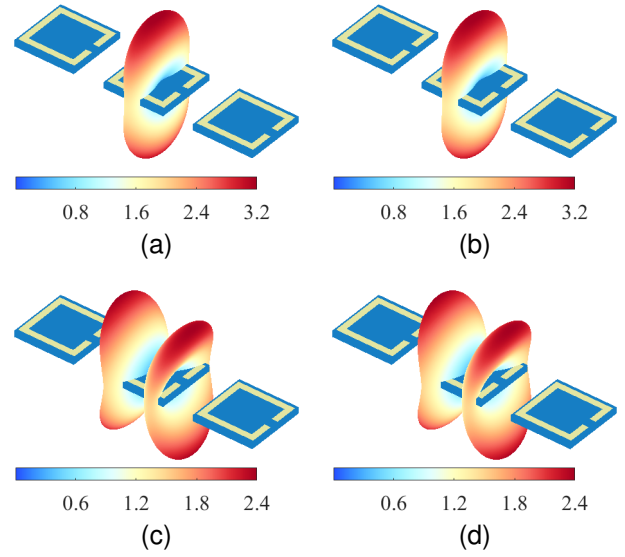


Fig. 10. Radiation patterns at 4.1 GHz. Panels (a) and (b) depict the first mode, while (c) and (d) depict the second mode. The left panels were obtained through full-wave simulation, and the right panels were generated using the synthesis method.

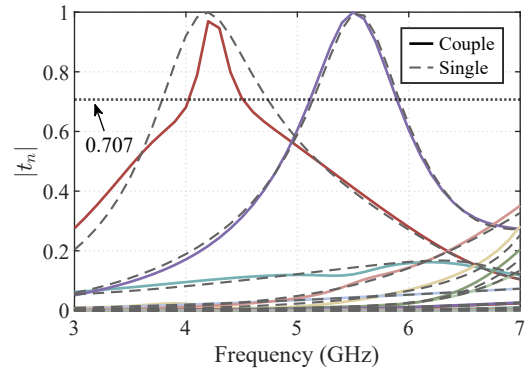


Fig. 11. Eigentraces. Lines labeled "Couple" account for array environment effects, while "Single" considers only the unit response. Generally, the 3 dB bandwidth of  $|t_n|$  reveals the practical working bandwidth, marked by a horizontal line at 0.707.

cell decreases by approximately 13% when coupling effects are considered. Notably, the primary radiation lobes of these two modes have split and no longer radiate directly broadside, as illustrated in Fig. 12. This observation underscores that the array's performance cannot be accurately analyzed or

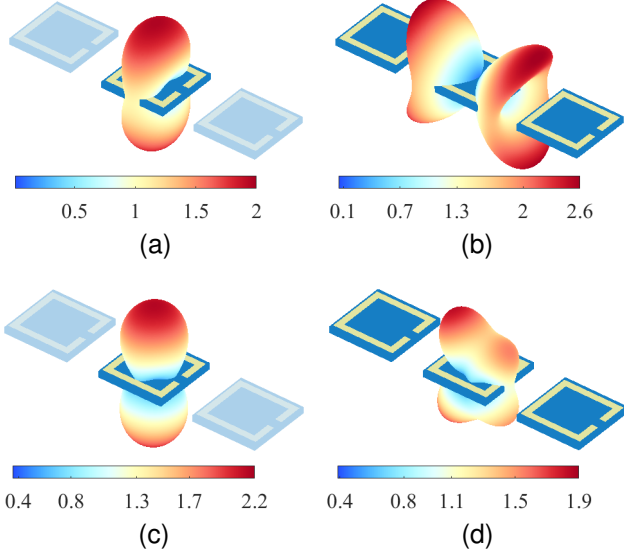


Fig. 12. (a), (b) are the radiation patterns of mode 1 at 4.2 GHz and (c), (d) are the patterns of mode 2 at 5.5 GHz. Note that (a) and (c) are the cases when the cell is alone, while (b) and (d) are when the cell is in the array environment but with the surrounding cells as background.

synthesized using the characteristic modes of an isolated cell in free space.

## VI. CONCLUSION AND DISCUSSION

This paper introduces a method to accelerate the decomposition of characteristic modes for structural combinations by utilizing T-matrices of individual structures. Our numerical results validate the method's accuracy and demonstrate its substantial computational advantages through the example of a 3-cell uniform array. Additionally, the analytical nature of the T-matrix for spheres allows for straightforward exploration of the variations in characteristic modes resulting from changes in the position and orientation of structures near spherical bodies, such as Earth.

While the T-matrix effectively relates the incident and scattering fields in the external region of any sphere circumscribing the structure, it does not account for the internal regions. Therefore, this study posits that different structures can be encapsulated within distinct, non-intersecting spheres. This realization underscores that further research is needed to develop methods for accelerating characteristic mode decomposition in tightly coupled arrays or structures in contact with one another.

### APPENDIX A

#### SCHUR COMPLEMENT METHOD

The Schur complement method is a powerful technique for solving matrix equations like

$$\mathbf{A}\mathbf{X} = \mathbf{B} \quad (14)$$

by utilizing the sub-blocks of the matrices involved.

Consider bifurcating (14) as

$$\begin{bmatrix} \mathbf{A}_{11} & \mathbf{A}_{12} \\ \mathbf{A}_{21} & \mathbf{A}_{22} \end{bmatrix} \begin{bmatrix} \mathbf{X}_1 \\ \mathbf{X}_2 \end{bmatrix} = \begin{bmatrix} \mathbf{B}_1 \\ \mathbf{B}_2 \end{bmatrix} \quad (15)$$

which gives the solution for  $\mathbf{X}_2 = \mathbf{A}_{22}^{-1} \{\mathbf{B}_2 - \mathbf{A}_{21}\mathbf{X}_1\}$ . This leads to a reduced equation for  $\mathbf{X}_1$ :

$$\tilde{\mathbf{A}}\mathbf{X}_1 = \tilde{\mathbf{B}} \quad (16)$$

where  $\tilde{\mathbf{A}} = \mathbf{A}_{11} - \mathbf{A}_{12}\mathbf{A}_{22}^{-1}\mathbf{A}_{21}$ ,  $\tilde{\mathbf{B}} = \mathbf{B}_1 - \mathbf{A}_{12}\mathbf{A}_{22}^{-1}\mathbf{B}_2$ . Collapsing these results, we have

$$\mathbf{X} = \mathbf{A}^{-1}\mathbf{B} = \begin{bmatrix} \mathbf{0} \\ \mathbf{A}_{22}^{-1}\mathbf{B}_2 \end{bmatrix} + \begin{bmatrix} \mathbf{1} \\ -\mathbf{A}_{22}^{-1}\mathbf{A}_{21} \end{bmatrix} \tilde{\mathbf{A}}^{-1}\tilde{\mathbf{B}}. \quad (17)$$

In the context of this paper, our objective is to determine the term  $(\mathbf{1} - \tilde{\mathbf{T}}\tilde{\mathbf{Y}})^{-1} \tilde{\mathcal{R}}^t$  in (10), where  $(\mathbf{1} - \tilde{\mathbf{T}}\tilde{\mathbf{Y}})$  serves as  $\mathbf{A}$  in (17), and  $\mathbf{A}_{22}$  contains matrices solely associated with background structures. In the process of calculating the background structures' T-matrix, the term  $\mathbf{A}_{22}^{-1}\mathbf{B}_2$  has been previously determined, necessitating only additional effort to find  $\tilde{\mathbf{A}}^{-1}$ . Note that the scale of  $\tilde{\mathbf{A}}^{-1}$  is relatively small, limited by the remaining structures after excluding the background structures.

### APPENDIX B

#### ROTATION MATRIX

There are many ways [18], [19] to express the element of the rotation matrix  $\mathcal{D}(\alpha, \beta, \gamma)$ , the most concise is in the form of matrix products:

$$\begin{aligned} \mathcal{D}_{nn'} &= \delta_{\tau\tau'} \delta_{ll'} \sqrt{\frac{\varepsilon_m \varepsilon_{m'}}{4}} (-1)^{m+m'} \\ &\times \begin{bmatrix} \cos(m\gamma) & \sin(m\gamma) \\ -\sin(m\gamma) & \cos(m\gamma) \end{bmatrix} \\ &\times \begin{bmatrix} A_{mm'}^l(\beta) & \\ & B_{mm'}^l(\beta) \end{bmatrix} \\ &\times \begin{bmatrix} \cos(m'\alpha) & \sin(m'\alpha) \\ -\sin(m'\alpha) & \cos(m'\alpha) \end{bmatrix} \end{aligned} \quad (18)$$

where the subscript  $n = \tau\sigma lm$  is a composite index [sca]. Note that  $\mathcal{D}_{nn'}$  is a scalar; thus, the appropriate element of the matrix product in (18) should be selected based on  $\sigma\sigma'$  index (*i.e.*,  $e/o$ ,  $e'/o'$ ). Here,  $\delta$  represents kronecker delta,  $\varepsilon_m = 2 - \delta_{m0}$ ,

$$\begin{aligned} A_{mm'}^l(\beta) &= d_{mm'}^l(\beta) + (-1)^{m'} d_{m-m'}^l(\beta) \\ B_{mm'}^l(\beta) &= d_{mm'}^l(\beta) - (-1)^{m'} d_{m-m'}^l(\beta) \end{aligned} \quad (19)$$

and the term  $d_{mm'}^l$  are defined as

$$\begin{aligned} d_{mm'}^l(\beta) &= \sqrt{\frac{(l+m)!(l-m)!}{(l+m')!(l-m')!}} \\ &\times \cos^{m+m'}\left(\frac{\beta}{2}\right) \sin^{m-m'}\left(\frac{\beta}{2}\right) \\ &\times P_{l-m}^{(m-m', m+m')}(\cos \beta) \end{aligned} \quad (20)$$

where  $P_n^{(a,b)}(x)$  denotes the Jacobi polynomials, typically computed using a three-term recurrence relation. Some useful properties include:

$$\begin{aligned} d_{mm'}^l(0) &= \delta_{mm'} \\ d_{mm'}^l(\pi) &= (-1)^{l+m'} \delta_{m-m'} \\ \mathcal{D}^{-1}(\alpha, \beta, \gamma) &= \mathcal{D}(-\gamma, -\beta, -\alpha) = \mathcal{D}^t(\alpha, \beta, \gamma) \\ \mathcal{D}(\alpha, \beta, \gamma) &= \mathcal{D}(\gamma) \mathcal{D}(\beta) \mathcal{D}(\alpha). \end{aligned} \quad (21)$$

## REFERENCES

- [1] M. Cabedo-Fabres et al., "The theory of characteristic modes revisited: A contribution to the design of antennas for modern applications," *IEEE Antennas Propag. Mag.*, vol. 49, no. 5, pp. 52-58, Oct. 2007.
- [2] M. Vogel, G. Gampala, D. Ludick, U. Jakobus, and C. J. Reddy, "Characteristic mode analysis: Putting physics back into simulation," *IEEE Antennas Propag. Mag.*, vol. 57, no. 2, pp. 307-317, Apr. 2015.
- [3] Y. Chen and C.-F. Wang, *Characteristic Modes: Theory and Applications in Antenna Engineering*, John Wiley & Sons, 2015.
- [4] J. L. T. Ethier and D. A. McNamara, "Sub-structure characteristic mode concept for antenna shape synthesis," *Electron. Lett.*, vol. 48, no. 9, pp. 1, 2012. *IEEE Antennas Propag. Mag.*, vol. 64, no. 2, pp. 23-31, Mar. 2022.
- [5] S. Huang, C. F. Wang, J. Pan, and D. Yang, "Accurate sub-structure characteristic mode analysis of dielectric resonator antennas with finite ground plan," *IEEE Trans. Antennas Propag.*, vol. 69, no. 10, pp. 6930-6935, Oct. 2021.
- [6] M. Capek and K. Schab, "Computational aspects of characteristic mode decomposition: An overview,"
- [7] S. Huang, C. F. Wang, and M. C. Tang, "Generalized surface-integral-equation-based sub-structure characteristic-mode solution to composite objects," *IEEE Trans. Antennas Propag.*, vol. 71, no. 3, pp. 2626-2639, Mar. 2023.
- [8] M. Gustafsson, L. Jelinek, K. Schab, and M. Capek, "Unified theory of characteristic modes—Part I: Fundamentals," *IEEE Trans. Antennas Propag.*, vol. 70, no. 12, pp. 11801–11813, Oct. 10, 2022.
- [9] C. Shi, J. Pan, et al., "Scattering-based characteristic mode theory for structures in arbitrary background: Computation, benchmarks, and applications," *IEEE Trans. Antennas Propag.*, 2024.
- [10] B. Peterson and S. Ström, "T matrix for electromagnetic scattering from an arbitrary number of scatterers and representations of E (3)," *Phys. Rev. D*, vol. 8, no. 10, pp. 3661, 1973.
- [11] D. W. Mackowski and M. I. Mishchenko, "Calculation of the T matrix and the scattering matrix for ensembles of spheres," *JOSA A*, vol. 13, no. 11, pp. 2266-2278, 1996.
- [12] J. Bruning and Y. Lo, "Multiple scattering of EM waves by spheres part I—Multipole expansion and ray-optical solutions," *IEEE Trans. Antennas Propag.*, vol. 19, no. 3, pp. 378-390, 1971.
- [13] D. W. Mackowski and M. I. Mishchenko, "A multiple sphere T-matrix Fortran code for use on parallel computer clusters," *J. Quant. Spectrosc. Radiative Transfer*, vol. 112, no. 13, pp. 2182-2192, 2011.
- [14] B. Friedman and J. Russek, "Addition theorems for spherical waves," *Q. Appl. Math.*, vol. 12, no. 1, pp. 13–23, 1954.
- [15] K. T. Kim, "The translation formula for vector multipole fields and the recurrence relations of the translation coefficients of scalar and vector multipole fields," *IEEE Trans. Antennas Propag.*, vol. 44, no. 11, pp. 1482–1487, Nov. 1996.
- [16] J. E. Hansen, Ed., *Spherical Near-Field Antenna Measurements*. London, U.K.: Peter Peregrinus Ltd., 1988.
- [17] G. Kristensson, *Scattering of Electromagnetic Waves by Obstacles*. Edison, NJ, USA: SciTech Publishing, 2016.
- [18] Z. Su and P. Coppens, "Rotation of real spherical harmonics," *Acta Crystallogr. A*, vol. 50, no. 5, pp. 636-643, 1994.
- [19] A. Boström, G. Kristensson, and S. Ström, "Transformation properties of plane, spherical and cylindrical scalar and vector wave functions," in *Acoustic, Electromagnetic and Elastic Wave Scattering, Field Representations and Introduction to Scattering*, Elsevier, 1991, pp. 165-210.